Hydrothermal Synthesis of Clove Buds-Derived Multifunctional Carbon Dots Passivated with PVP- Antioxidants, Catalysis, and Bioimaging Applications

Anurag Kumar Pandey [a], Kamakshi Bankoti [b], Tapan Kumar Nath [c], Santanu Dhara [b *]

[a] School of Nano Science and Technology, Indian Institute of Technology Kharagpur, Kharagpur, West Bengal – 721302

[b] School of Medical Science and Technology, Indian Institute of Technology Kharagpur, Kharagpur, West Bengal – 721302

[c] Department of Physics, Indian Institute of Technology Kharagpur, Kharagpur, West Bengal – 721302

[*] Corresponding author

Prof. Santanu Dhara (Professor) School of Medical Science and Technology IIT Kharagpur 721302, West Bengal., India Email: sdhara@smst.iitkgp.ac.in Phone: +91-3222-282306

Abstract

The present study reports a one-step clean synthesis of carbon dots (CDs) using clove buds and polyvinylpyrrolidone (PVP) as the starting precursor via hydrothermal routes. The adopted technique is facile, reproducible, and cost-effective for the production of externally passivated carbon dots owing to an environmentally friendly process utilizing natural precursors. The study evidenced the synergetic effect of passivation on light absorption and fluorescence properties in comparison to non-passivated carbon dots (CCDs). The structural and morphological study revealed that the PVP-passivated clove-derived carbon dots (PPCCDs) were spherical with an average diameter of ~ 2 nm and crystalline with an interlayer spacing of 0.33 nm. The PPCCDs showed excellent antioxidant activity against DPPH free radicals and also showed good catalytic activity for the degradation of Rhodamine-B (Rh-B) dye under studied conditions. Synthesized PPCCDs showed dose-dependent toxicity in L929 (mouse fibroblast) cell lines, while the appropriate concentration used in biological studies was found to be biocompatible as evidenced by MTT assays and also revealed in bioimaging potential. To conclude, synthesised PPCCDs is an economically potent candidate with multifunctional aspects, which can serve as an excellent antioxidant, catalyst, and efficient multicolor bioimaging tool.

Keywords: Clove Buds; PVP-Passivated Carbon Dots; Hydrothermal; Antioxidant; Catalysis; Bioimaging

1. INTRODUCTION

The reticence in widespread applicability of nanotechnology is associated with various issues regarding the environmental hazard, and unknown health-related issues associated with high surface energy and usage of heavy metal ions. In this regard, carbon-based materials have been recognized as effective nanomaterials in terms of availability and minimal toxicity. During the past two decades, various carbon nanostructures with different physicochemical properties have been inspected due to their distinct shapes and sizes, with several known allotropes and structures of carbon [1]. Among them, carbon dots (CDs) have fascinated great interest since their astonishing properties along with safety and efficacy were explored by refinement of single-walled carbon nanotubes (SWNTs) [2]. Their superior versatility in properties of photoluminescence, electron donor/acceptor ability, and photo-bleaching in comparison to traditional quantum dots or metallic nanocrystals makes them the most promising in the fields of bio-labeling, free radical scavenging, catalysis, solar cells, metal ion sensors, and many more [3–9].

The selection of synthesis techniques and precursors for CDs set a benchmark for its applicability in various fields. There are various techniques reported for carbonization and fabrication of CDs such as laser ablation, combustion, pyrolysis, hydrothermal, and microwave irradiation, etc. [10–16]. Herein, the hydrothermal route is most efficient due to its simplicity, low process cost, and controllable reaction conditions [3]. The carbon sources or precursors for CDs synthesis can be classified as either man-made or natural [5]. Among them, natural carbon sources are investigated more fascinatingly because of their low-cost, nontoxic behavior, and convenience. The reaction precursors are a crucial factor in deciding the photophysical and

photochemical properties of CDs along with their applicability. The search for new carbon precursors at low cost, natural or less damaging, and environmentally favorable is still desirable. Multifunctionality aspects of CDs can be attained using two adapted techniques, viz. doping and surface passivation. These techniques involve the inclusion of dopant atoms in the core and the attachment of functional groups over the surface of CDs intrinsically or extrinsically. Intrinsic passivation depends totally on carbon precursors, while extrinsic passivation uses external agents to modify the surface of CDs. Extrinsic passivation is beneficial in terms of adding new functionality in nanomaterials. It is used to improve the aqueous stability, surface properties, and optoelectronic properties of CDs with extensions in their application ranges. In recent years, various polymers such as PAA, PEI, PEG, and TTDDA have been used with natural or man-made sources as passivating agents for CDs synthesis [12–16]. But the multifunctionality aspect of CDs still needs to be surveyed to verify their potential as smart nanomaterials without compromising their simplicity and toxicity. However, to our best knowledge, there is no significant study on the synthesis of PVP-passivated carbon dots derived from clove buds along with their diverse applications.

By keeping sight of the aforementioned issues, we are reporting a one-pot hydrothermally synthesis of polyvinylpyrrolidone (PVP) passivated carbon dots (PPCCDs) derived from clove buds as a green resource. This strategy is simple, economical, time-saving, eco-friendly, and uses only water as a solvent in comparison to other passivation techniques reported so far [13,14]. Clove buds (*Syzygium aromaticum*) belong to the family of Myrtaceae, which is a tropical plant that grows mainly in the southern part of India. Aqueous extract of clove buds is used for the treatment of dyspepsia and gastric irritation and is also reported as a very good antibacterial and antioxidant agent [17,18]. PVP is a non-toxic, water-soluble, biocompatible polymer used as a surface stabiliser in the synthesis of

nanomaterials, pharmaceuticals, the food industry, and biomedicine [19,20]. So, due to PVP passivation with nitrogen as a dopant, these CDs can enhance their multifunctionality aspects with diversity in applications. In this article, we have analyzed the physicochemical and optoelectronic properties of synthesized PPCCDs. Furthermore, our study also inspects the multifunctional facets of PPCCDs in various applications such as free radical scavenging over DPPH assay, catalysis over the degradation of organic dye Rh-B in presence of sodium borohydride ($NaBH_4$) as a reducing agent, and bioimaging using the L929 cell line.

2. MATERIALS AND METHODS

The floral clove buds were purchased from a local grocery store of the Indian Institute of Technology Kharagpur, West Bengal, India. Dimethyl sulfoxide (DMSO), 3-(4,5-dimethylthiazol-2-yl)-2,5-diphenyltetrazolium Bromide (98%) (MTT), Butylated hydroxytoluene (BHT), Nitro blue tetrazolium chloride (NBT), and 2, 2-diphenyl-1-picrylhydrazyl (DPPH) were procured from Sigma-Aldrich. Sodium chloride, Ethylenediaminetetraacetic acid (EDTA), hydrogen peroxide (H_2O_2), potassium dihydrogen phosphate, and disodium hydrogen phosphate were purchased from Merk, India. Polyvinylpyrrolidone (PVP) and Rhodamine-B (Rh-B) were bought from Sisco research laboratory Pvt. Ltd (SRL), India. The L929 cell was procured from NCCS, Pune, India. Deionized water was used for all synthesis reactions and analysis of CDs.

2.1 Synthesis of CDs- The purchased clove buds were washed thrice with distilled water to eliminate dust particles, followed by drying in a hot air oven overnight at 100 °C. The raw material was then grounded into fine powder utilizing the mortar and pestle. Then, 0.5 g of fine clove powder with and without PVP (polyvinylpyrrolidone) was dispersed in 30 mL of water with continuous stirring and heating at 100 °C for 30 min using a mechanical stirrer (REMI,

India). The resultant homogenous reaction mixture was transferred to a 60 ml capacity autoclave chamber (TECHNISTRO, India) at 200 °C for 5 h in the hot air oven. The larger particles in the supernatant were separated through centrifugation for 15 min at 10,000 rpm followed by filtering through a 0.22-micron syringe filter (Sartorius, India). The filtrate containing PPCCDs was dried and reconstituted to a 10 mg/mL solution and stored at 4 °C for further experiments.

2.2 Characterization of CDs

CDs were systematically characterized to study their physicochemical properties that will further define their biological and non-biological applications. To analyze the functional groups, present in PPCCDs, CCDs, and PVP Fourier Transform Infrared spectroscopy (FTIR) was performed by drop-casting and drying samples on KBr pellets using Nicolet 6700 (Thermo Fischer Scientific Instruments, USA). UV-Visible spectrometer 201 (Thermo Scientific, USA) was used to analyze the absorption spectra of synthesized samples. The fluorescent property was analyzed using spectrofluorometer RF-6000 series (Shimadzu, India). The nanostructure of PPCCDs was analyzed employing high-resolution transmission electron microscopy (JEM-2100 HR-TEM, JEOL, Japan) with 200kV accelerating voltage. In brief, the sample was drop cast on a carbon-coated copper grid with overnight drying at 25 °C to get rid of remnant moisture. The histogram for size distribution calculation representing the average particle size was plotted over 100 particles count using Image J software. For elemental composition profiling of PPCCDs, X-ray photoelectron spectroscopy (XPS, PHI 5000Verse Probe II (ULVAC-PHI Inc., Japan)) was performed.

2.3 Stability study of PPCCDs

The fluorescence intensity dependency on pH and UV light exposure are two key factors to investigate the stability of fluorescent dye and also ensure their applicability in biological environments. In brief, the aqueous solution of PPCCDs (0.05 mg/mL) was used with HCl (2M) or NaOH (2M) to adjust their pH, either acidic or alkaline. The same amount of PPCCDs was also studied for the different exposure times of UV light (254 nm). The effect of pH variation and UV light exposure on fluorescence and absorption intensity was investigated using Fluorescence and UV-Visible spectroscopy.

2.4 Antioxidant activity assay

2.4.1 DPPH free radical assay

The *ex vivo* antioxidant efficacy of PPCCDs was evaluated by a DPPH assay with minor modifications [21]. The presence of an antioxidant molecule scavenges DPPH free radicals, reducing purple-colored stable radical cation to a yellow-colored solution with a consequent decrease or loss of absorbance, which can be measured via a UV-Vis spectrophotometer.

In brief, 0.3 ml of methanolic solution of DPPH (0.5mM) was added to different concentrations of the sample PPCCDs and standard BHT and incubated in the dark for 100 min. The optical density post-reaction completion was measured using a UV-Vis spectrophotometer at 517 nm. The experiment was repeated thrice with 5 batches of PPCCDs to ensure reproducibility. The antioxidant efficacy against the DPPH free radical was calculated using the following equation:

$$\textbf{Antioxidant activity (\%)} = \frac{A_{Control} - A_{PPCCDs}}{A_{Control}} \times 100 \qquad (1)$$

2.4.2 Superoxide radical assay

The superoxide radical scavenging assay was performed using the NBT assay with minor modification [22]. The reaction mixture of sodium carbonate (125mM, pH 10.2), NBT (24 µM), EDTA (0.1mM), and hydroxylammonium chloride (1mM) without catalyst was taken as control. The reaction was initiated by adding different concentrations of PPCCDs in the above reaction mixture and recording the optical density at 560 nm after 30 minutes of incubation using a spectrophotometer. The superoxide inhibition percentage was calculated using the following equation.

$$\textbf{Superoxide radical inhibition (\%)} = \frac{A_{Control} - A_{PPCCDs}}{A_{Control}} \times 100 \qquad (2)$$

2.4.3 H_2O_2 degradation study

The CAT-mimicking activity of PPCCDs was evaluated by recording the change in OD of H_2O_2 at 240 nm. The reaction mixture contains 50 µL of PPCCDs with phosphate-buffered saline buffer (100mM, pH 7.2), and H_2O_2 (43 mM) to make a final volume of 3mL. The reaction mixture without PPCCDs was taken as a control. For blank, the same amount of PPCCDs in PBS was added without H_2O_2 to avoid auto-absorbance at 240 nm due to PPCCDs. The percentage of residual H_2O_2 in the reaction mixture was calculated using the following equation.

$$\textbf{Residual } H_2O_2 \textbf{ (\%)} = \frac{A_{Control} - A_{PPCCDs}}{A_{Control}} \times 100 \qquad (3)$$

2.5 Investigation of catalytic activity

The catalytic activity of PPCCDs was evaluated over the degradation of Rhodamine-B (Rh-B) in the presence of sodium borohydride ($NaBH_4$) using the UV-Vis spectrophotometer. The reactants and catalyst concentration were established by following the modified protocol [6]. Briefly, two cuvettes each of 3.5 mL capacity were occupied with 0.20 mL of newly prepared

$NaBH_4$ (0.50 M), 1 mL of Rh-B (0.01mM), and 1.8 mL of water to make up to 3 mL complete solution. One of the above cuvettes was added with 20 µL (0.2 mg/mL) of PPCCDs, while the other served as a control for the study. The degradation of Rh-B was examined by capturing the time-dependent absorbance of the reaction mixture at 554 nm wavelength using UV-Visible spectroscopy after every 2 minute time interval. The degradation percentage (%) of Rh-B dye was calculated as per Eq. 4.

$$\textbf{\% Degradation} = \frac{A_0 - A_t}{A_t} \times 100 \qquad \textbf{(4)}$$

Where A_0 is the initial absorbance at time t = 0, and A_t stands for the absorbance after reaction time t.

2.6 Evaluation of cytotoxicity

The toxicity of PPCCDs was evaluated using the MTT assay, wherein mitochondrial succinic dehydrogenase enzymes present in actively proliferating cells will reduce tetrazolium compound (MTT dye) into its insoluble purple color formazan crystal. In brief, L929 cells were seeded in 96 well plates at a cell density of 5000 cells/well in complete DMEM, high glucose media (Thermo Fischer Scientific, USA) containing Fetal bovine serum (10% FBS, Thermo Fischer Scientific, USA), and antimycotic-antibacterial (1%, Thermo Fischer Scientific, USA). A series of diluted concentrations of PPCCDs, i.e., 0.1, 0.3, 0.5, 0.7, 0.9, and 1.1 mg/mL were added to each well in triplicate post-48 h incubation in an incubator maintained at 37 °C, 5% CO_2, and 95% humidity. After 48 h of treatment, the MTT reagent (5 µg/mL) was added in the dark environment and incubated for 4 h more. After incubation, an equivalent amount of DMSO was added to solubilize the purple formazan crystals, and the optical density was evaluated at 570 nm

using the BIO-RAD microplate reader-550. The untreated cells were taken as a control for the study and processed similarly. The cell viability was evaluated using the following equation:

$$\textbf{Cell viability (\%)} = \frac{A_{570\,Control} - A_{570\,PPCCDs}}{A_{Control}} \times 100 \qquad (5)$$

2.7 Live cell imaging

For assessing the bioimaging potential of PPCCDs, L929 cells (5000 cells/coverslip) were cultured on a poly-L-lysine-coated coverslip and incubated in a culture medium containing PPCCDs for 9 h. Subsequently, the cultured cells were repeatedly washed with PBS to avoid any overstaining before being captured under the inverted fluorescence microscope (eclipse Ts2R-FL, Nikon, Japan). The coverslip was imaged with the help of fluorescence microscopy in bright field and fluorescence mode.

3. RESULTS AND DISCUSSION

PVP-passivated carbon dots (PPCCDs) were successfully synthesized from clove buds using hydrothermal carbonization at 200 °C for 5 h, as depicted in **Fig. S1**. The colors of non-passivated CCDs and passivated PPCCDs carbon dots were observed to be light yellow or dark greyish-black under white light respectively, while under UV light illumination, both CDs showed green fluorescence as shown in **Fig. S2**. The quantum yield of CCDs and PPCCDs were performed and calculated to be 7.6% and 10.9%, as shown in **Fig. S4**. This dictates the surface passivation of PVP results in improved quantum yield in comparison to non-passivated carbon dots (**Table S1**). The quantum yield and multifunctional aspects of various surface passivated

carbon dots are compared in **Table S4.** The PPCCDs solution was darker when compared with the CCDs, which may be due to the passivation of CCDs owing to the addition of PVP.

3.1 Physiochemical characterization of CDs

3.1.1 FTIR analysis- FTIR analysis of CCDs, PPCCDs, and pure PVP (**Fig. 1a**) were studied for analysis of the functional groups and bonds associated with CDs. The FTIR spectrum of PPCCDs demonstrating broadband in the range 3600-3200 cm^{-1} belongs to the stretching vibration of the O-H group and hydrogen-bonded N-H group [23]. Two smaller peaks at 2922 $cm^{-1}$and 2862 cm^{-1} represent symmetric and asymmetric vibration of the $-CH_3$ and $-CH_2$ groups. The presence of sp^2 hybridized honeycomb lattice (aromatic C = C or C = O stretching) is indicated by a sharp peak at 1645 cm^{-1} in the case of pure PVP and PPCCDs, which have redshift for CCDs. The absorption peak at wavenumber 1287.6 cm^{-1} belongs to the C-N bond stretching in PVP [24]. The peak at 1050 cm^{-1} is ascribed to the stretching vibration bands of C-O on the PPCCDs surface, while the peak at 1027 cm^{-1} resembles the aromatic ether group present due to PVP addition [25]. The FTIR spectrum of PPCCDs represents the combination of various bond and functional groups present in pristine PVP (dissolve in water) and CCDs spectrum collectively. The presence of functional groups at the surface of CDs makes them well dispersed in water.

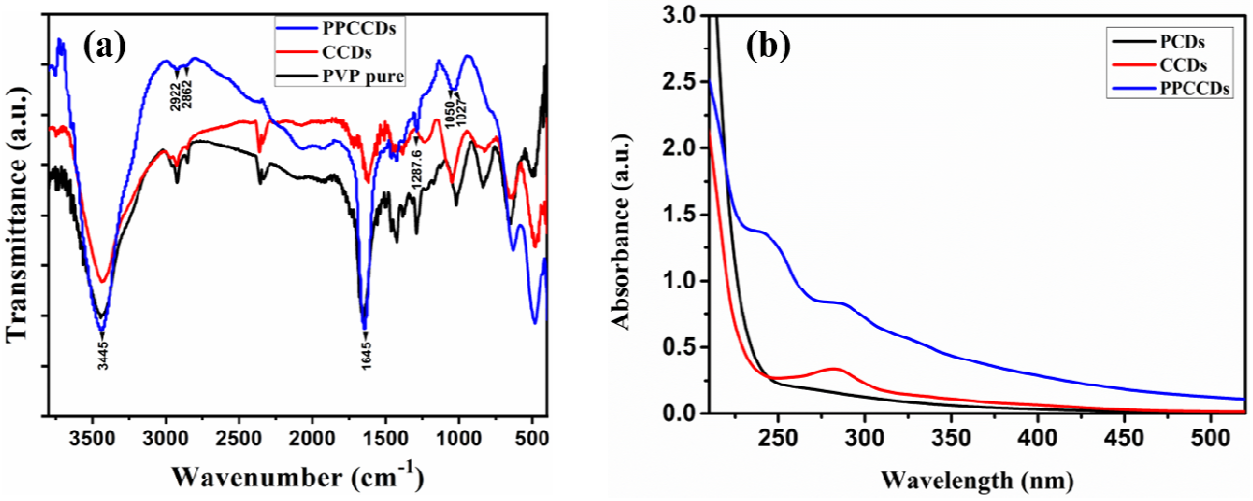

Fig. 1. (a) FTIR spectra and (b) UV-Vis absorption spectra of passivated (PPCCDs) and non-passivated (CCDs) carbon dots, along with bare PVP FTIR (a) and (b) UV-Vis spectrum of PVP derived carbon dot (PCDs).

3.1.2 Optical behavior of CDs.

The photophysical analysis of non-passivated (CCDs), PVP derived CDs (PCDs), and passivation (PPCCDs) carbon dots was performed to understand their optical behavior and the synergistic effect of passivation collectively. **Fig. 1b** indicates UV-Vis analysis of PPCCDs and CCDs with two broad absorption peaks at 288 nm and 282 nm, respectively, belongs to π–π* electron transition of C=C bonds [6]. While one more small shoulder peak at 324 nm in the PPCCDs sample resembles n–π* electron transition of C=O bonds [3,6]. For comparison, the UV-Vis spectrum of carbon dots derived from PVP (PCDs) as shown in **Fig. 1b** indicates absorption in the deep ultraviolet region. The surface passivation is responsible for an increase in absorption intensity (in the wavelength range of 240-600 nm) of passivated CDs in contrast to

the non-passivated CDs [26]. The comparative study of the fluorescent behavior of CCDs, PCDs, and PPCCDs as shown in **Fig. 2ace** revealed a significant difference in their fluorescent emission by varying the excitation wavelength in the range of 340-500 nm with a 20 nm increment. The passivated PPCCDs have three coexisting emission peaks centered at 415 nm, 439 nm, and 462 nm in comparison to non-passivated CCDs at 432 nm, which attained their maxima when excited at 380 nm and 360 nm excitation wavelengths, respectively. While PCDs is showing maximum emission at 417 nm when excited by 340 nm wavelength. Specifically, the fluorescence peaks at 432 nm for CCDs and 417 nm for PCDs was shifted at 439 nm and 415 nm, respectively, in the case of PPCCDs. Notably, an additional peak at 462 nm has appeared in the case of PPCCDs as a result of passivation that might be due to the synergistic effect. Pal et al. also reported a similar result for CDs derived from curcumin while passivated by polyethyleneimine [14]. They have shown the synergistic effect on the fluorescence behavior of passivated CDs as compared to the CDs derived from their native ones. As shown in **Fig 2bdf**, samples were excited within the wavelength range of 340 nm to 500 nm, PCDs had emission at a regular interval, while CCDs had relatively different phenomena. Initially, peaks of emission spectra at the excitation wavelength range of 340 to 380 nm had marginal differences while spectra at 380 nm and above a relatively higher magnitude of peak shift was observed. Interestingly, this clustering effect of emission spectra for CCDs was further evident in the case of PPCCDs as a result of passivation with PVP. The multiple emission peaks of PPCCDs show both types of fluorescent characteristics, such as excitation independent emission at and below 400 nm wavelength and excitation dependent emission above 400 nm excitation wavelength, similar to reported literature [27,28]. The unique uniform surface emissive trap of passivated CDs at lower wavelengths is valuable for avoiding autofluorescence issues and is also responsible for excitation independent

emission [27]. While the excitation wavelength-dependent emission behavior of CDs is outcome of the various surface emissive traps with different energy levels at a higher wavelengths [28]. One possible explanation for coexisting peaks is the occurrence of different electron transitions inside the graphitic core as a result of different size effects and surface defects in passivated CDs [29,30]. The photophysical properties of PPCCDs are more efficient and improved than CCDs and were further studied and explored for multiple applications.

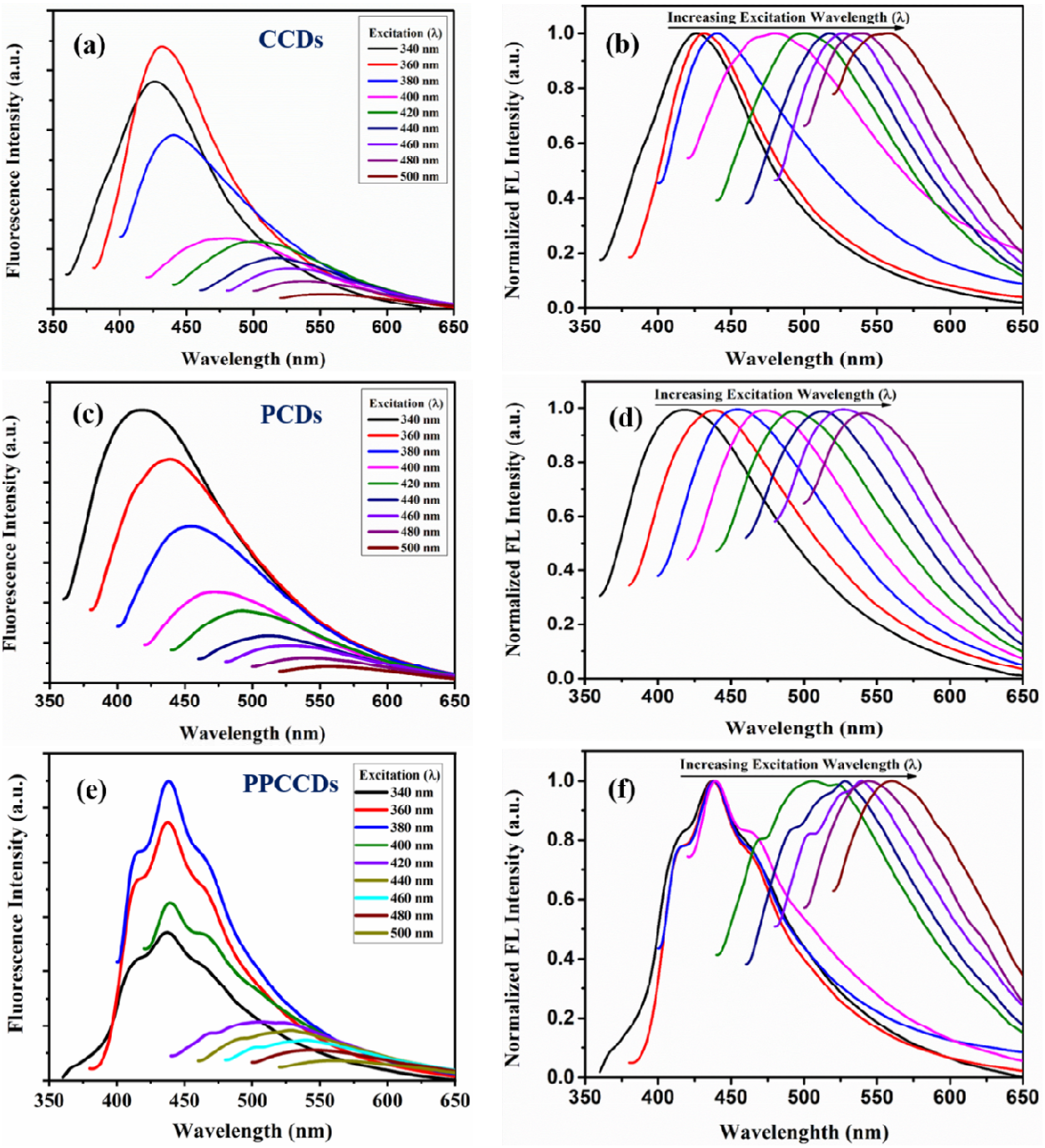

Fig.2. (a, c, and e) representing fluorescent emission spectra, and (b, d, and f) showing normalized fluorescent spectra of CCDs, PCDs, and PPCCDs carbon dots by varying the excitation wavelength in the range of 340-500 nm.

3.1.3 Morphological, Structural and Chemical characterization. The structural and morphological analysis shown in **Fig. 3** represents the XRD data, TEM images, carbon dots size distribution, and HRTEM images of PPCCDs. The XRD analysis reveals one broad peak at 2θ =

23.54°, which corresponds to the (002) plane of graphitic carbon of crystalline nature [31]. In the case of CCDs, the XRD peak is a little shifted to 24.4° as shown in **Fig S5a**. While TEM images demonstrate the spherical shape of PPCCDs with an average diameter of 2 nm. The histogram plot was obtained by using image-J software which resembled different size particles with a size distribution window in the range of 1-5 nm. The HRTEM image showed lattice fringes with a d spacing value of around 0.33 nm, indicating the presence of (002) plane of the graphitic carbon validated with XRD data. The TEM analysis of CCDs showed the presence of agglomerated carbon dots, as shown in **Fig S5b,** that were mostly stabilized after passivation.

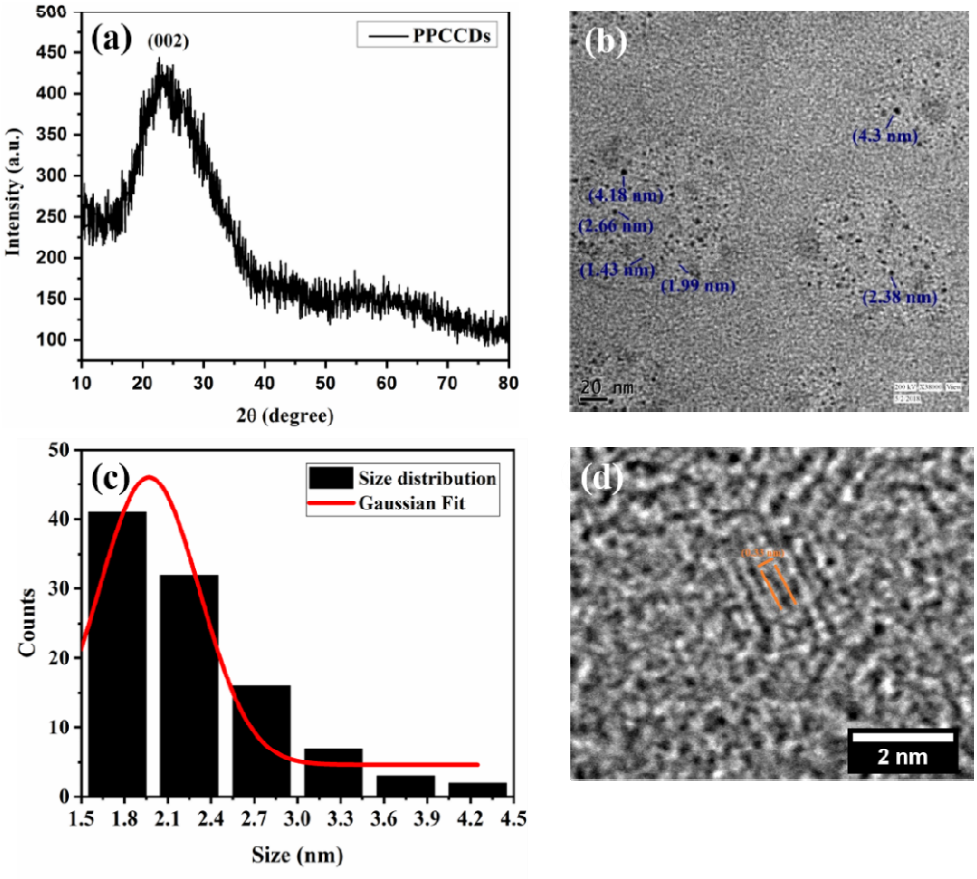

Fig. 3. (a) XRD spectrum, (b) TEM image, (c) respective size distribution histogram, and (d) HRTEM fringe pattern image of PPCCDs.

X-ray photoelectron spectroscopy (XPS) was accomplished to further examine the surface chemical state and composition of PPCCDs. The clove buds mostly contain eugenol and eugenol acetate as major components dictating the presence of hydrogen, carbon, and oxygen elements in their chemical structure [32,33]. The full scan spectrum as shown in **Fig. 4a** revealed the existence of carbon, oxygen, and nitrogen, atoms peak with an atomic ratio of 85.30%, 10.50%, and 4.20%, respectively.

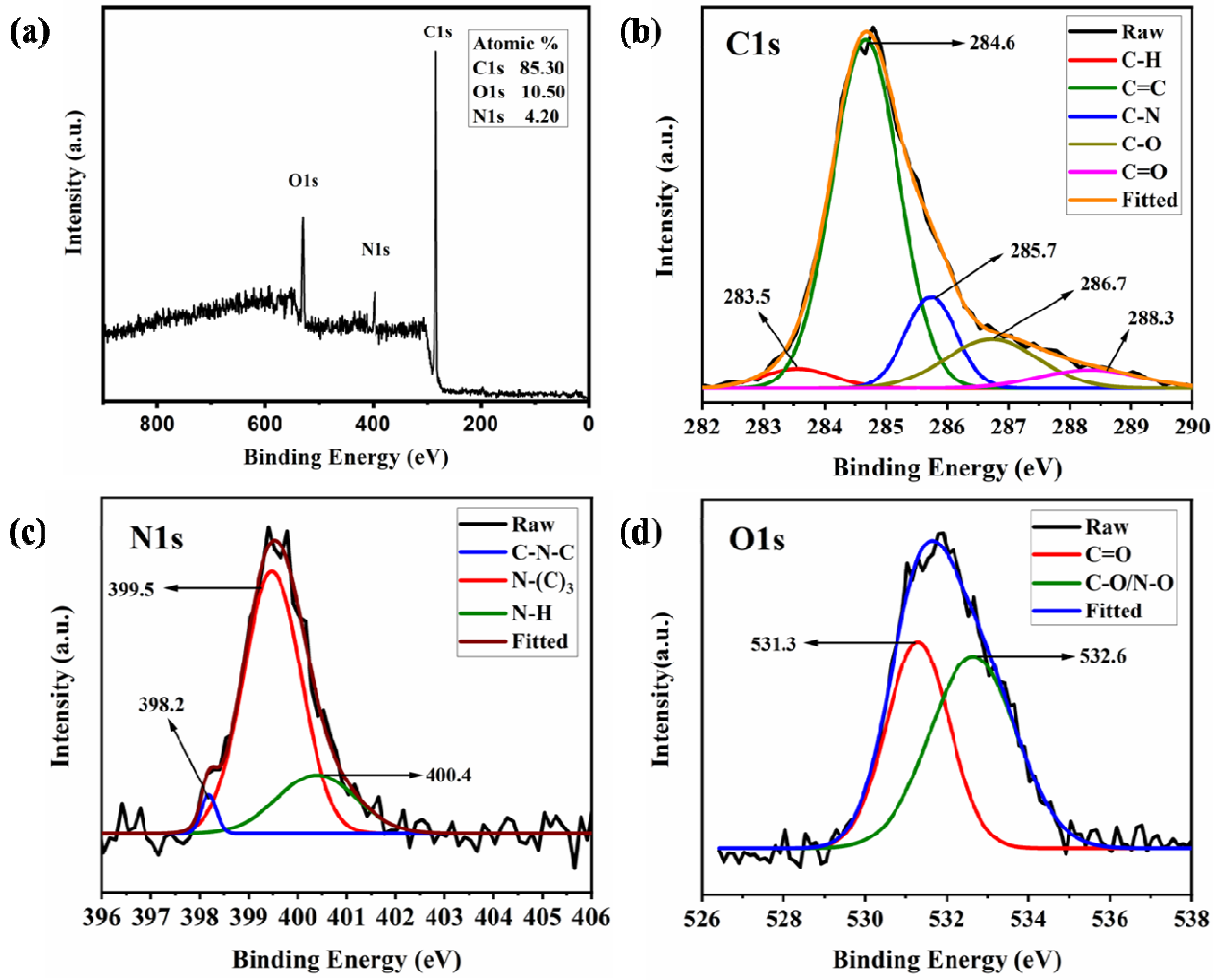

Fig. 4. (a) The full scan XPS spectrum and HR-XPS spectrum of (b) $C1_s$, (c) $N1_s$, and (d) $O1_s$ of synthesized carbon dots (PPCCDs).

High-resolution spectra of $C1_s$, $N1_s$, and $O1_s$ as shown in **Fig. 4b-d** validate the presence of various atomic bonds validation with FTIR data. The deconvoluted $C1_s$ spectrum revealed the presence of C-H, C=C, C-N, C-O, and C=O bonds with their respective binding energies of 283.5, 284.6 eV, 285.7 eV, 286.7 eV, and 288.3eV [14,23]. Furthermore, the deconvoluted spectrum of the $N1_s$ peak shown in **Fig. 4c** revealed three peaks at 398.2 eV, 399.5 eV, and 400.4 eV that are associated with the functionality of the C-N-C, pyrrolic N, and N-H bonds, correspondingly, confirm the presence of nitrogen doping in CDs [14,31]. While **Fig. 4d** revealed deconvoluted $O1_s$ spectrum with two peaks at 531.3 eV and 532.6 eV belong to C=O, C-O/N-O bonds, respectively [34].

3.2 Stability of PPCCDs

The effect of pH and ultraviolet light irradiation on PPCCDs were performed to establish their stability under the studied conditions. As shown in **Fig. 5a,** pH variation does not have any significant change in the absorption intensity and spectra of PPCCDs, revealing the absence of aggregation in the studied conditions. The fluorescence spectrum was also observed with a corresponding change in pH values. Interestingly, at pH 7 the fluorescence spectra showed a similar intense band equivalent to the intensity at pH 11 supporting its suitable applicability for live-cell imaging as shown in **Fig. 5b.** Further, the impact of bleaching on PPCCDs has also been assessed post UV exposer over 3 h. As shown in **Fig. 5c-d,** there was no significant change in peaks intensity or position for both absorption and fluorescence spectra revealing post UV exposure PPCCDs neither aggregated nor lost their intensity significantly beneath understudied conditions.

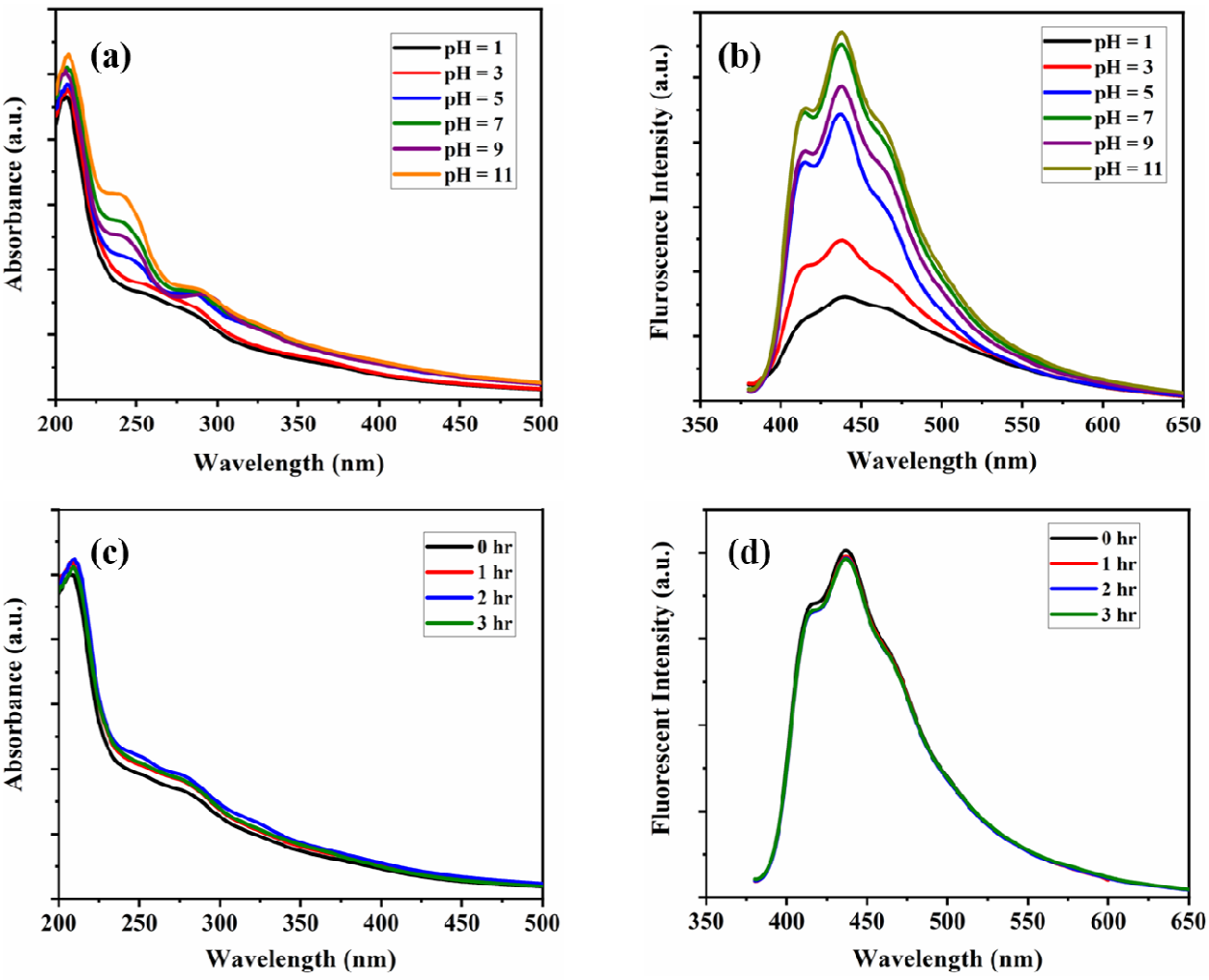

Fig. 5. (a) and (c) represent UV-Visible spectra, (b) and (d) showing the fluorescent spectra of variant pH (in range 1-11) and ultraviolet exposer (λ= 254 nm) of the PPCCDs sample: Excitation wavelength for fluorescence emission was 360 nm.

3.3 Antioxidant activity

The major problem regarding the generation of reactive oxygen species or free radicals in biological systems could be scavenged or neutralized by nanomaterials having good antioxidant activity [21,35–38]. The CDs have both electron donors and acceptors capability that makes them act as good antioxidant and prooxidant agents [39,40]. The CDs are a less explored and more suitable candidate for antioxidant study due to their minimal toxicity [3,4,31].

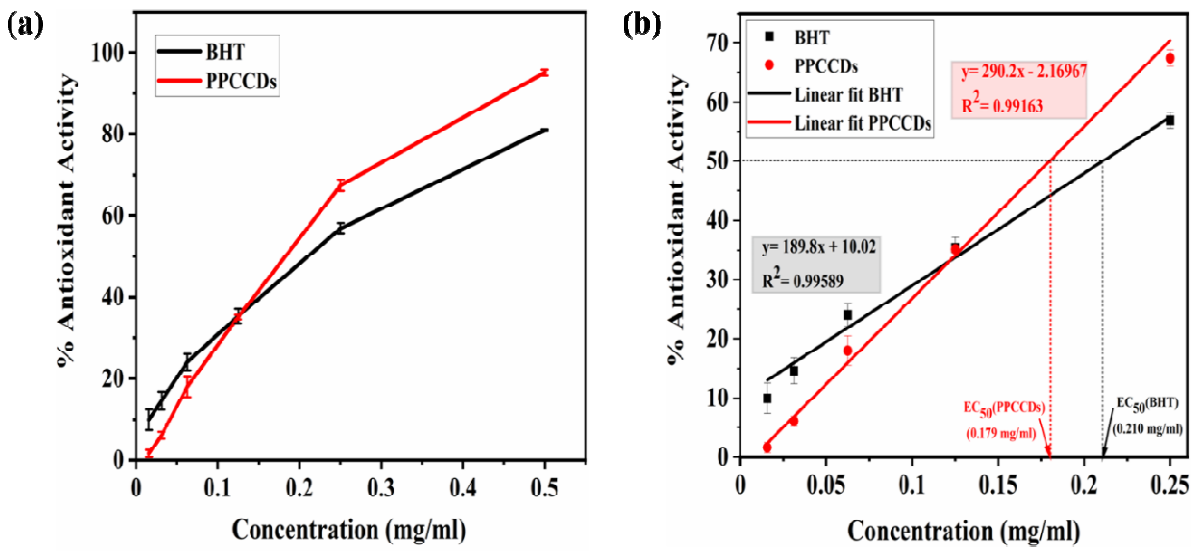

Fig. 6. (a) Antioxidant activity of PPCCDs and BHT over DPPH assay at different concentrations and (b) linear fitting of antioxidant activity with their EC_{50} value.

The antioxidant efficacy of PPCCDs was measured by using a standard DPPH free radical assay. It was noticeably detected from **Fig. 6a** that PPCCDs have superior antioxidant efficacy (94%) when compared to BHT (81%) at the highest concentration of 0.5 mg/mL. The inhibition efficacy increased with an increase in concentration for both BHT and PPCCDs. The antioxidant activity of PPCCDs and BHT both show an approximately linear relationship with concentration up to 0.25 mg/mL with an R^2 value of 0.99. The results as shown in **Fig. 6b** represent the EC_{50} (concentration required to reduce 50% of the original DPPH free radical) value of PPCCDs (0.179 mg/mL), which was lower as compared to the EC_{50} of standard BHT (0.210 mg/mL). The lower EC_{50} value of PPCCDs signifies that it is more potent at scavenging DPPH free radicals than standard BHT taken for the study and hence, has better antioxidant potential. The antioxidant efficacy of PPCCDs toward DPPH radical degradation was found to be superior in comparison to other reported carbon dots as shown in **Table S2**.

Superoxide radical scavenging activity

The superoxide radical scavenging activity of PPCCDs was performed using an NBT assay. The mechanism involves the generation of superoxide anion by auto-oxidation of hydroxylammonium chloride while maintaining sodium carbonate at basic pH 10.2. The generated superoxide anion in the presence of a catalyst inhibits the reduction of NBT. The UV-Vis spectrum as shown in **Fig. 7a** indicated the superoxide radical scavenging potential of PPCCDs at different concentrations. As the concentrations of PPCCDs increased, there was a decrease in absorption intensity at 560 nm that indicated the inhibition of formazan formation with concentration. While **Fig. 7b** represents the percentage of superoxide radical inhibition with a change in concentrations, indicating SOD-mimicking ability of as-prepared carbon dots. The superoxide radical inhibition of 89% acquired at a concentration of 0.5 mg/mL along with an EC_{50} value of 105 µg/mL calculated from **Fig 7b** is comparable or better than other reported literature shown in **Table S2** [4,21,41].

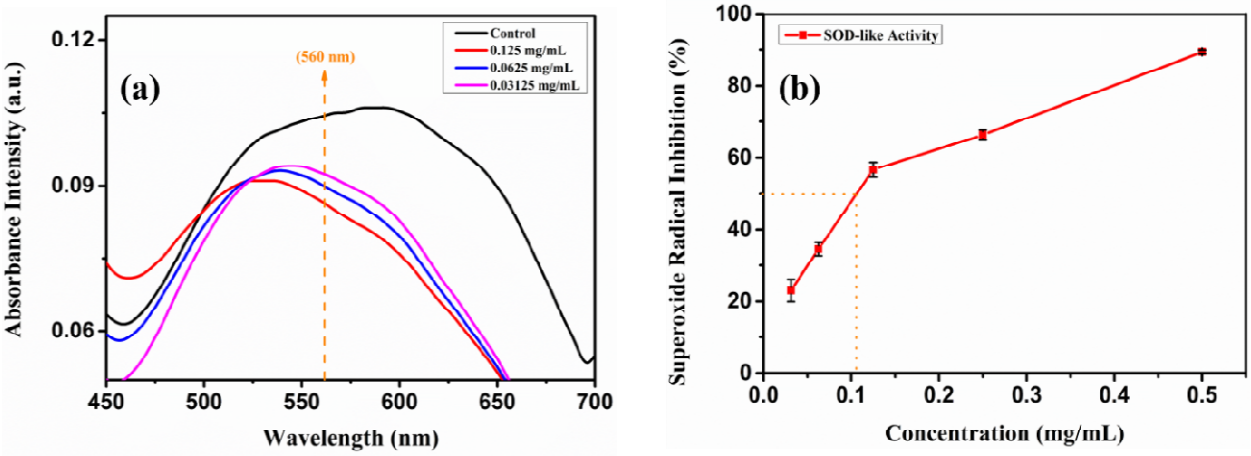

Fig.7 (a) NBT reduction inhibition absorption spectra and (b) superoxide radical inhibition activity plotted against increasing PPCCD concentrations.

Hydrogen peroxide degradation study

The ability of nanomaterials to reduce hydrogen peroxide to oxygen and water plays an important role in inhibiting ROS formation inside or outside the cells, also known as catalase-mimic potential [42,43]. The CAT-mimic study of PPCCDs with time was performed by monitoring the decrease in absorbance value of H_2O_2 at 240 nm using a UV-Vis spectrophotometer. **Fig. 8a** shows a clear picture of the change in absorbance at 240 nm concerning time using a 1mg/mL concentration of PPCCDs. The residual H_2O_2 percentage plot vs time as shown in **Fig. 8b** indicates that within 30 minutes, 16% of H_2O_2 (43mM) was catalyzed in the presence of PPCCDs. While without a catalyst, very little decrease was observed in the same time frame of 30 minutes. This reduction of H_2O_2 absorbance at 240 nm with the function of time indicated the CAT-mimicking capability of nanomaterial [44].

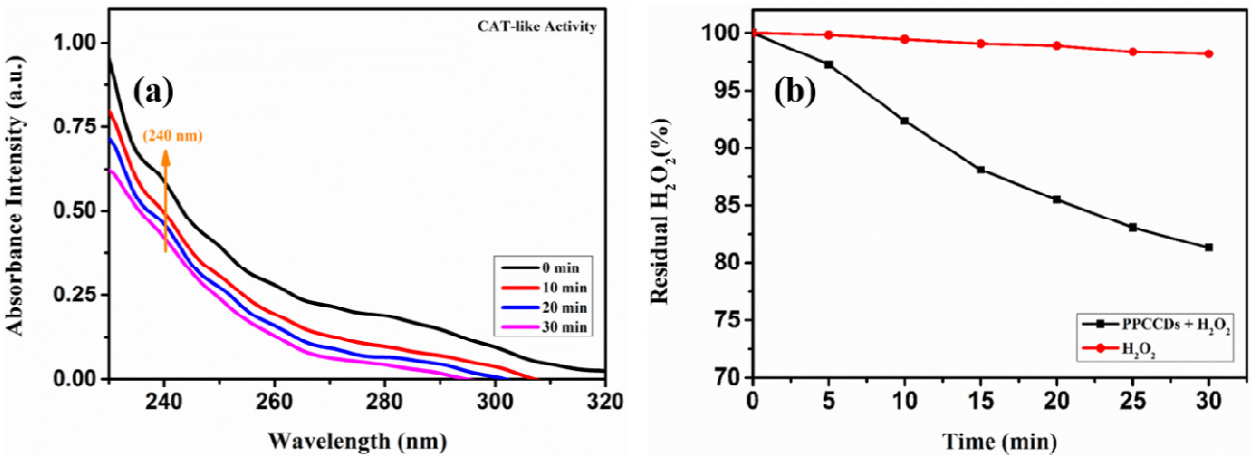

Fig. 8. (a) The absorption spectra of H_2O_2 degradation with concentration changes; and (b) the plot of residual H_2O_2 percentage over 30-minute time frame in the presence and absence of PPCCDs.

3.4 Catalytic activity over Rh-B In this study, Rh-B as a modal pollutant was designated to inspect the catalytic activity of PPCCDs using $NaBH_4$ as a reducing agent. Rh-B is a commercialized organic dye most efficiently used in the textile, leather, and biological industry. It harm the environment and human health when disposed of in river water as waste without pre-treatment. Its accumulation in water results in various neurotoxic, mutagenic, and reproductive health issues in both animals and humans [45]. So, the demand for simple and cost-effective techniques along with efficient and non-toxic catalyst material is desirable for the removal of organic dyes from wastewater.

The aqueous solution of Rh-B shows a pink-red color with a characterized maximum absorption peak at a wavelength of 554 nm. **Fig. 9** represents the reduction of Rh-B using $NaBH_4$ with/without the addition of PPCCDs as a catalyst for 20 minutes along with their degradation and rate kinetics. It can be demonstrated from **Fig. 9a-b** that the peak intensity of Rh-B dye decreased more gradually with time after adding $NaBH_4$ alone in comparison to adding $NaBH_4$ in the presence of PPCCDs. Hence, PPCCDs addition to the reaction mixture stimulated the degradation of dye as observed by a significant reduction in absorbance intensity. The plot of reaction kinetics of dye degradation with/without catalysts was evaluated by monitoring the change in absorbance concerning reaction time. The dye degradation kinetics were studied and found to have a first-order linear relationship, as described by the equation:

$$ln \frac{A}{A0} = - k_{app} \times t \qquad (3)$$

Here, A_0 and A are the absorbance at times t = 0 and t, k_{app} = apparent rate constant, and t = reaction time.

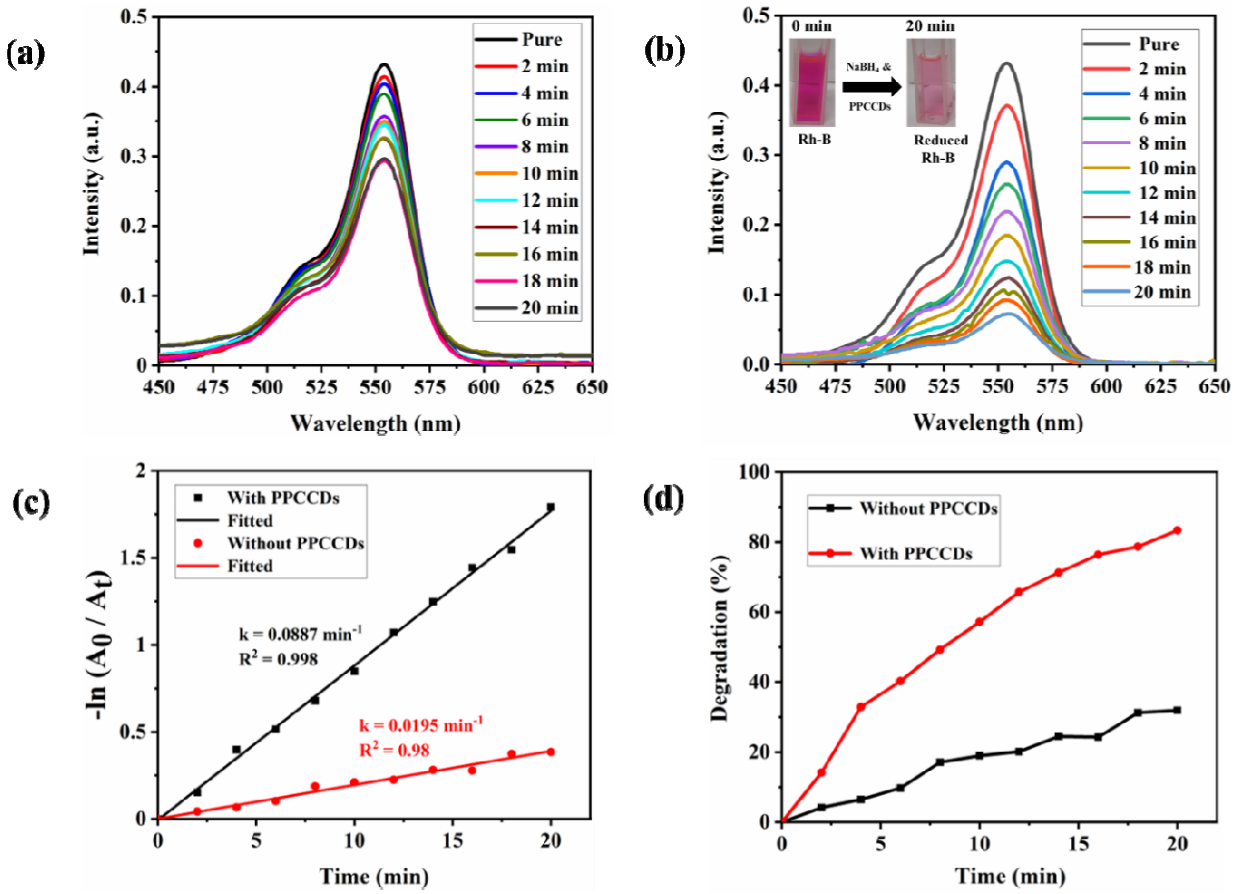

Fig. 9. (a) and (b) showing reduction of Rh-B captured by UV-Visible spectroscopy, (c) reaction kinetics plot, and (d) representing degradation plot of Rh-B dye using $NaBH_4$ with/without adding PPCCDs. Inset in Fig. 9b shows decolorization of Rh-B in the presence of PPCCDs as a catalyst.

The linear dependency of ln (A/A_0) concerning time as shown in **Fig. 9c** confirms first-order rate kinetics of the reaction with an apparent rate constant of 0.0887 and 0.0195 min^{-1} with R^2 values of 0.998 and 0.98 in the presence and absence of catalyst, respectively. The specific rate constant was calculated by dividing the apparent rate constant k_{app} with the mass of catalyst (m) used, $k' = k_{app}/m$ in mg. The specific rate constant of PPCCDs was calculated to be 7.39 s^{-1} g^{-1}. The specific rate constant k and apparent rate constant k_{app} of PPCCDs was found to be superior when compared with some other reported catalysts shown in **Table S3** [46–50]. The presence of

PPCCDs results in faster degradation of Rh-B dye by nearly 86% **(Fig. 9d)** within 20 minutes, showing that the synthesized PPCCDs have good catalytic activity in the studied conditions.

The CDs due to their small size and high surface-to-volume ratio could be projected as an effective substrate for dye degradation. The process of degradation of Rh-B dye using PPCCDs as catalysts in the presence of $NaBH_4$ can be better understood by the Langmuir-Hinshelwood mechanism represented in Fig. 10.

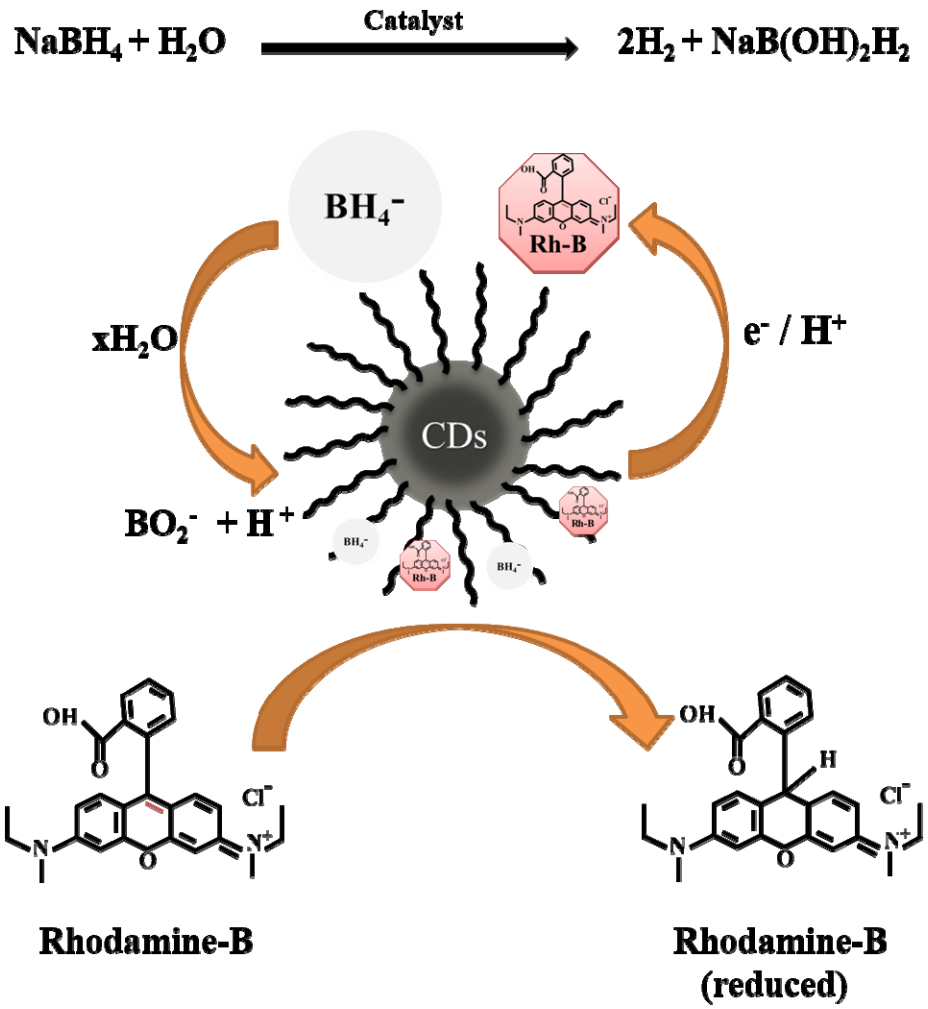

Fig. 10. Schematic of the chemical reaction and process mechanism of Rh-B dye degradation using $NaBH_4$ as a reducing agent and carbon dots as a catalyst.

The reaction mechanism involves the oxidation of an aqueous solution of sodium borohydride in the presence of CDs as a catalyst liberates hydrogen bubbles [51]. The borate ions (BH_4^-) adsorb over the surface of catalysts oxidized with water molecules to generate BO_2^- ions and protonated hydrogen atoms. The role of the catalyst here is to decrease the reductive potential of $NaBH_4$ and increase the reductive potential of Rh-B dye due to their nucleophilic and electrophilic nature. Further, the Rh-B dye and borate ions (BH_4^-) are adsorbed over the surface of CDs acting as a moderator (electron relay system) to receive an electron from borate ions and hand over the electron back to Rh-B through its surface [6]. Breaking of the conjugated system in the molecule and decrease of the potential barrier between reactant and product by evolving continuous H_2 gas bubbles during this reduction reaction are explained in **Fig. 10**. The pink colors of Rh-B decolorized to colorless due to the destruction of the dye chromophore structure into less toxic species. Hence, the large surface-to-volume ratio due to smaller size and efficient electron-accepting potential due to nitrogen doping might be reasons which are credited with the good catalytic activity of PPCCDs.

3.5 In-vitro Cytotoxicity Test

Low cytotoxicity is one of the most important requirements for bio-imaging agents, and a big drawback of semiconductor QDs employed in biomedical areas. Hence, to recognize the potential cytotoxicity of the PPCCDs, an MTT assay was performed using L929 and 3T3 cells. **Fig. 11 and Fig. S7** showed that the cell viability of PPCCDs for both cell lines was more than 80% after 48 h of treatment with a PPCCDs solution at the concentration of 0.5 mg/ml, and a remarkable decrease in cell viability was observed when higher doses of PPCCDs were employed. These observations signify that PPCCDs is a feasible candidate for cellular imaging in biomedical applications when used in appropriate concentrations.

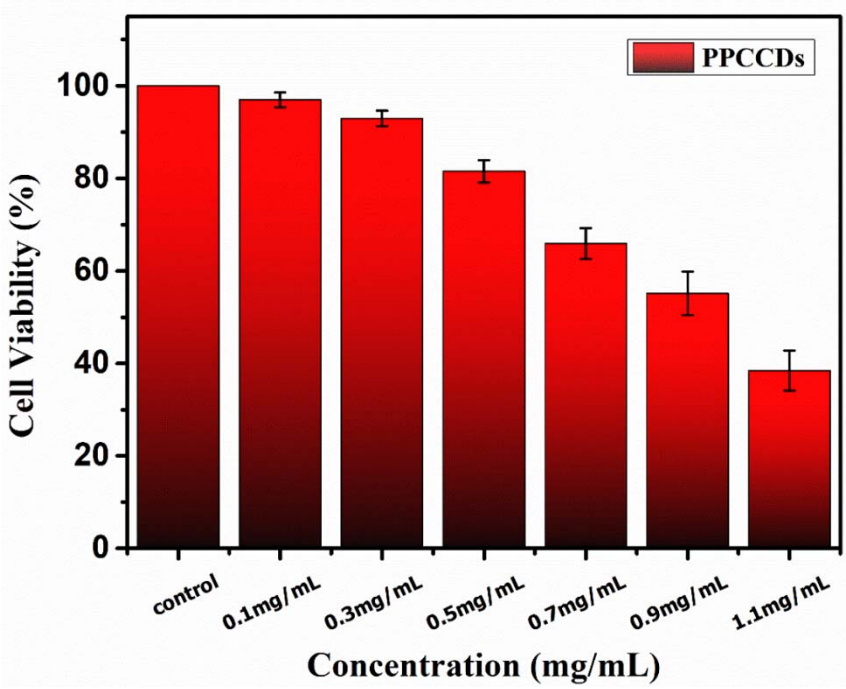

Fig. 11. Cytotoxic evaluation of prepared concentrations of PPCCDs using MTT assay on fibroblast cells after 48 h incubation.

3.6 Live-cell imaging experiment

The bright-field and respective multicolor fluorescent images of L929 cells treated with PPCCDs at the different excitation wavelengths of 405 (blue), 488 (green), and 542 nm (red) were captured using a fluorescent microscope as shown in **Fig. 12**. The optimized concentration of PPCCDs for staining fibroblast cells was 0.25 mg/mL. The close investigation revealed that PPCCDs was more efficiently taken up by the cell membrane and cytoplasm region, as evident by thestrong fluorescence. The possible mechanism for the entry of PPCCDs inside the cell could be due to endocytosis. The untreated fibroblast cells (without PPCCDs labeling) as shown in **Fig. S3** was found to be non-emissive when excited by lasers of wavelength 405 nm, 488 nm, and 542 nm, respectively. The results are similar to previous literature in which CDs have been demonstrated to stain cytoplasm and cell membrane [31,52]. The multicolor imaging capability

of PPCCDs is better than various previously reported carbon dots[3,26,53,54]. This signifies that the synthesized PPCCDs could serve as an efficient bioimaging tool.

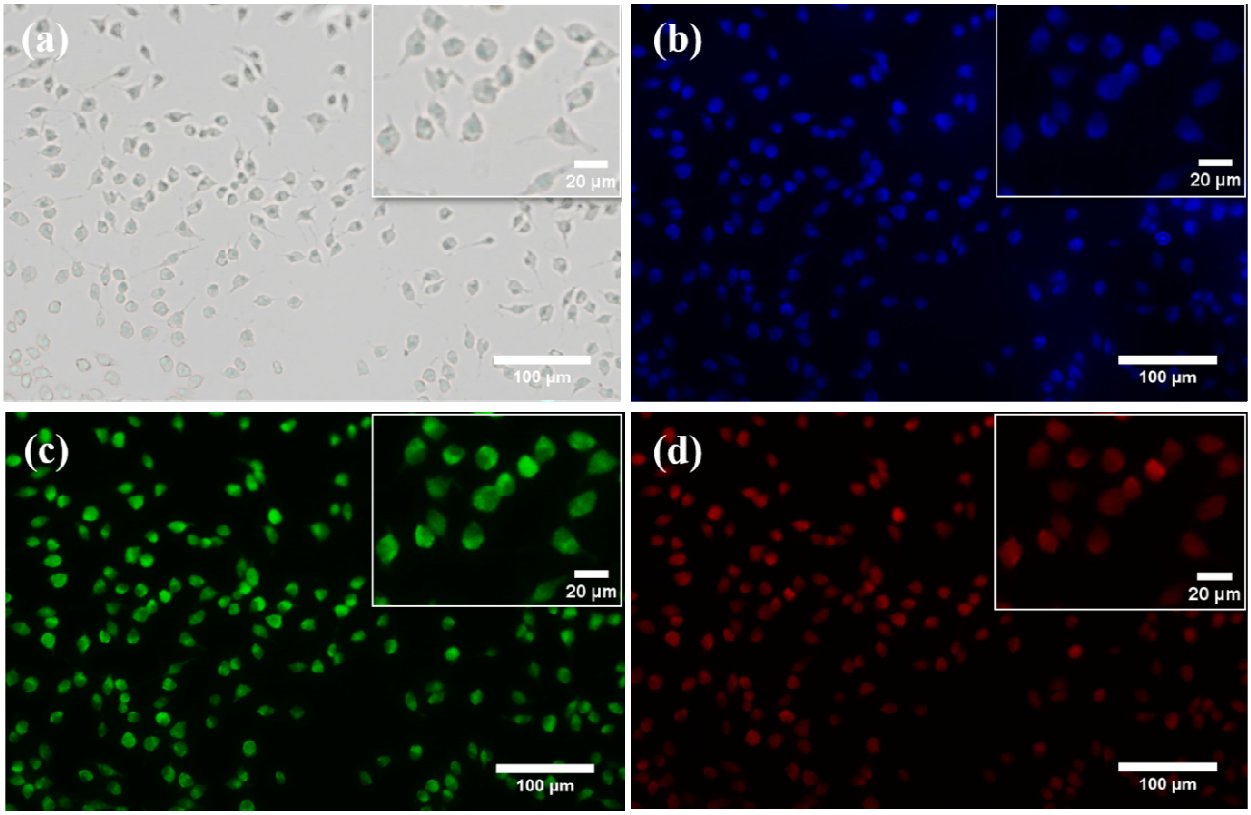

Fig. 12. The fluorescent microscopy images representing in (a) bright-field and (b-d) fluorescent imaging of L929 cells incubated with synthesized PPCCDs (0.25mg/mL) for 9 h. The fluorescent images were captured at an excitation wavelength of (b) 405nm, (c) 488nm, and (d) 542nm. Scale bar: 100 µm. Inset shows magnified images at Scale bar: 20 µm.

4. CONCLUSION

The cost-effective synthesis of surface passivated clove-derived carbon dots via the hydrothermal method has been reported in this article. The optical study was performed over CCDs and PPCCDs to understand the effects of passivation on their photophysical properties. The as-synthesized PPCCDs have excitation independent emission at a lower wavelength that is pivotal to avoid autofluorescence. The structural and morphological studies were performed to confirm the formation of spherical and graphitic carbon dots with a diameter of ~ 2 nm. The photostability and pH stability tests were performed that demonstrated the insignificant effect of UV exposure on PPCCDs emission for biological applications. The cytocompatibility test of PPCCDs has shown more than 85% cell viability up to concentrations of 0.25 mg/mL using fibroblast cells making them a potential candidate for bioimaging. PPCCDs was effectively taken up by L929 cells and confined mainly to the cytoplasm and cell membrane regions, highlighting their potential as fluorescence imaging nanoprobes. Synthesized PPCCDs demonstrated excellent antioxidant activity (EC_{50} = 0.179 mg/mL), even superior to standard BHT (EC_{50} = 0.210 mg/mL) taken for the study. PPCCDs showed prominent catalytic activity in the degradation of the organic dye Rh-B using $NaBH_4$. Overall, PPCCDs was synthesized by an economically viable process to serve as an efficient bioimaging tool, an excellent antioxidant, and a good catalyst.

Acknowledgment

The authors would like to thank MHRD (Ministry of human resource development), India for fellowship support and CRF (Central research facility), IIT Kharagpur for physiochemical characterizations. The authors are grateful to SNST, SMST, the Department of Physics, and the Department of Chemistry for their valuable contributions to the analysis.

References

[1] V. Georgakilas, J.A. Perman, J. Tucek, R. Zboril, Broad Family of Carbon Nanoallotropes: Classification, Chemistry, and Applications of Fullerenes, Carbon Dots, Nanotubes, Graphene, Nanodiamonds, and Combined Superstructures, Chem. Rev. 115 (2015) 4744–4822. https://doi.org/10.1021/cr500304f.

[2] X. Xu, R. Ray, Y. Gu, H.J. Ploehn, L. Gearheart, K. Raker, W.A. Scrivens, Electrophoretic Analysis and Purification of Fluorescent Single-Walled Carbon Nanotube Fragments, J. Am. Chem. Soc. 126 (2004) 12736–12737. https://doi.org/10.1021/ja040082h.

[3] A. Sachdev, P. Gopinath, Green synthesis of multifunctional carbon dots from coriander leaves and their potential application as antioxidants, sensors and bioimaging agents, Analyst. 140 (2015) 4260–4269. https://doi.org/10.1039/C5AN00454C.

[4] K. Bankoti, A.P. Rameshbabu, S. Datta, B. Das, A. Mitra, S. Dhara, Onion derived carbon nanodots for live cell imaging and accelerated skin wound healing, J. Mater. Chem. B. 5 (2017) 6579–6592. https://doi.org/10.1039/C7TB00869D.

[5] X. Zhang, M. Jiang, N. Niu, Z. Chen, S. Li, S. Liu, J. Li, Natural-Product-Derived Carbon Dots: From Natural Products to Functional Materials, ChemSusChem. 11 (2018) 11–24. https://doi.org/10.1002/cssc.201701847.

[6] V. Arul, T.N.J.I. Edison, Y.R. Lee, M.G. Sethuraman, Biological and catalytic applications of green synthesized fluorescent N-doped carbon dots using Hylocereus undatus, J. Photochem. Photobiol. B Biol. 168 (2017) 142–148. https://doi.org/10.1016/j.jphotobiol.2017.02.007.

[7] M. Sabet, K. Mahdavi, Green synthesis of high photoluminescence nitrogen-doped carbon quantum dots from grass via a simple hydrothermal method for removing organic and inorganic water pollutions, Appl. Surf. Sci. 463 (2019) 283–291. https://doi.org/10.1016/j.apsusc.2018.08.223.

[8] Q. Yang, J. Duan, W. Yang, X. Li, J. Mo, P. Yang, Q. Tang, Nitrogen-doped carbon quantum dots from biomass via simple one-pot method and exploration of their application, Appl. Surf. Sci. 434 (2018) 1079–1085. https://doi.org/10.1016/j.apsusc.2017.11.040.

[9] D. Gu, S. Shang, Q. Yu, J. Shen, Green synthesis of nitrogen-doped carbon dots from lotus root for Hg(II) ions detection and cell imaging, Appl. Surf. Sci. 390 (2016) 38–42. https://doi.org/10.1016/j.apsusc.2016.08.012.

[10] Y.-P. Sun, B. Zhou, Y. Lin, W. Wang, K.A.S. Fernando, P. Pathak, M.J. Meziani, B.A. Harruff, X. Wang, H. Wang, P.G. Luo, H. Yang, M.E. Kose, B. Chen, L.M. Veca, S.-Y. Xie, Quantum-Sized

Carbon Dots for Bright and Colorful Photoluminescence, J. Am. Chem. Soc. 128 (2006) 7756–7757. https://doi.org/10.1021/ja062677d.

[11] S. Zhang, L. Zhang, L. Huang, G. Zheng, P. Zhang, Y. Jin, Z. Jiao, X. Sun, Study on the fluorescence properties of carbon dots prepared via combustion process, J. Lumin. 206 (2019) 608–612. https://doi.org/10.1016/j.jlumin.2018.10.086.

[12] L.-H. Mao, W.-Q. Tang, Z.-Y. Deng, S.-S. Liu, C.-F. Wang, S. Chen, Facile Access to White Fluorescent Carbon Dots toward Light-Emitting Devices, Ind. Eng. Chem. Res. 53 (2014) 6417–6425. https://doi.org/10.1021/ie500602n.

[13] Y. Hao, Z. Gan, J. Xu, X. Wu, P.K. Chu, Poly(ethylene glycol)/carbon quantum dot composite solid films exhibiting intense and tunable blue–red emission, Appl. Surf. Sci. 311 (2014) 490–497. https://doi.org/10.1016/j.apsusc.2014.05.095.

[14] T. Pal, S. Mohiyuddin, G. Packirisamy, Facile and Green Synthesis of Multicolor Fluorescence Carbon Dots from Curcumin: In Vitro and in Vivo Bioimaging and Other Applications, ACS Omega. 3 (2018) 831–843. https://doi.org/10.1021/acsomega.7b01323.

[15] C. Liu, P. Zhang, F. Tian, W. Li, F. Li, W. Liu, One-step synthesis of surface passivated carbon nanodots by microwave assisted pyrolysis for enhanced multicolor photoluminescence and bioimaging, J. Mater. Chem. 21 (2011) 13163. https://doi.org/10.1039/c1jm12744f.

[16] N. Arsalani, P. Nezhad-Mokhtari, E. Jabbari, Microwave-assisted and one-step synthesis of PEG passivated fluorescent carbon dots from gelatin as an efficient nanocarrier for methotrexate delivery, Artif. Cells, Nanomedicine, Biotechnol. 47 (2019) 540–547. https://doi.org/10.1080/21691401.2018.1562460.

[17] C.H. Mina Kumari, I. Bhaskar Reddy, K. Vijaya Rachel, Free radical scavenging and antioxidant activity of methanol extract of Syzygium aromaticum, Biosci. Biotechnol. Res. Asia. 7 (2010) 833–840.

[18] K.-G. Lee, T. Shibamoto, Antioxidant property of aroma extract isolated from clove buds [Syzygium aromaticum (L.) Merr. et Perry], Food Chem. 74 (2001) 443–448. https://doi.org/10.1016/S0308-8146(01)00161-3.

[19] K.M. Koczkur, S. Mourdikoudis, L. Polavarapu, S.E. Skrabalak, Polyvinylpyrrolidone (PVP) in nanoparticle synthesis, Dalt. Trans. 44 (2015) 17883–17905. https://doi.org/10.1039/C5DT02964C.

[20] M. Kurakula, G.S.N.K. Rao, Pharmaceutical assessment of polyvinylpyrrolidone (PVP): As excipient from conventional to controlled delivery systems with a spotlight on COVID-19 inhibition, J. Drug Deliv. Sci. Technol. 60 (2020) 102046. https://doi.org/10.1016/j.jddst.2020.102046.

[21] B. Das, P. Dadhich, P. Pal, P.K. Srivas, K. Bankoti, S. Dhara, Carbon nanodots from date molasses: New nanolights for the in vitro scavenging of reactive oxygen species, J. Mater. Chem. B. 2 (2014) 6839–6847. https://doi.org/10.1039/c4tb01020e.

[22] Y. Kono, Generation of superoxide radical during autoxidation of hydroxylamine and an assay for superoxide dismutase, Arch. Biochem. Biophys. 186 (1978) 189–195. https://doi.org/10.1016/0003-9861(78)90479-4.

[23] P. Huang, S. Xu, M. Zhang, W. Zhong, Z. Xiao, Y. Luo, Modulation doping of absorbent cotton derived carbon dots for quantum dot-sensitized solar cells, Phys. Chem. Chem. Phys. 21 (2019) 26133–26145. https://doi.org/10.1039/C9CP04880D.

[24] S. Selvam, M. Sundrarajan, Functionalization of cotton fabric with PVP/ZnO nanoparticles for improved reactive dyeability and antibacterial activity, Carbohydr. Polym. 87 (2012) 1419–1424. https://doi.org/10.1016/j.carbpol.2011.09.025.

[25] T. Gutul, E. Rusu, N. Condur, V. Ursaki, E. Goncearenco, P. Vlazan, Preparation of poly(N -vinylpyrrolidone)-stabilized ZnO colloid nanoparticles, Beilstein J. Nanotechnol. 5 (2014) 402–406. https://doi.org/10.3762/bjnano.5.47.

[26] A. Sachdev, I. Matai, S.U. Kumar, B. Bhushan, P. Dubey, P. Gopinath, A novel one-step synthesis of PEG passivated multicolour fluorescent carbon dots for potential biolabeling application, RSC Adv. 3 (2013) 16958. https://doi.org/10.1039/c3ra42415d.

[27] Y. Zhang, P. Cui, F. Zhang, X. Feng, Y. Wang, Y. Yang, X. Liu, Fluorescent probes for “off–on” highly sensitive detection of Hg2+ and L-cysteine based on nitrogen-doped carbon dots, Talanta. 152 (2016) 288–300. https://doi.org/10.1016/j.talanta.2016.02.018.

[28] Y. Zhai, X. Bai, H. Cui, J. Zhu, W. Liu, T. Zhang, B. Dong, G. Pan, L. Xu, S. Zhang, H. Song, Carbon dot/polyvinylpyrrolidone hybrid nanofibers with efficient solid-state photoluminescence constructed using an electrospinning technique, Nanotechnology. 29 (2018) 025706. https://doi.org/10.1088/1361-6528/aa99be.

[29] J. Ren, F. Weber, F. Weigert, Y. Wang, S. Choudhury, J. Xiao, I. Lauermann, U. Resch-Genger, A. Bande, T. Petit, Influence of surface chemistry on optical, chemical and electronic properties of blue luminescent carbon dots, Nanoscale. 11 (2019) 2056–2064. https://doi.org/10.1039/C8NR08595A.

[30] S. Wang, I.S. Cole, D. Zhao, Q. Li, The dual roles of functional groups in the photoluminescence of graphene quantum dots, Nanoscale. 8 (2016) 7449–7458. https://doi.org/10.1039/C5NR07042B.

[31] S. Zhao, M. Lan, X. Zhu, H. Xue, T.W. Ng, X. Meng, C.S. Lee, P. Wang, W. Zhang, Green Synthesis of Bifunctional Fluorescent Carbon Dots from Garlic for Cellular Imaging and Free

Radical Scavenging, ACS Appl. Mater. Interfaces. 7 (2015) 17054–17060. https://doi.org/10.1021/acsami.5b03228.

[32] G.A. Ayoola, T. Adelowotan, I. Aibinu, E. Adenipekun, Chemical analysis and antimicrobial activity of the essential oil of Syzigium aromaticum (clove), African J. Microbiol. Res. 2 (2008) 162–166. https://doi.org/10.5897/AJMR.9000161.

[33] A.A. Khalil, U.U. Rahman, M.R. Khan, A. Sahar, T. Mehmood, M. Khan, Essential oil eugenol: sources, extraction techniques and nutraceutical perspectives, RSC Adv. 7 (2017) 32669–32681. https://doi.org/10.1039/C7RA04803C.

[34] V. Ramanan, B. Siddaiah, K. Raji, P. Ramamurthy, Green Synthesis of Multifunctionalized, Nitrogen-Doped, Highly Fluorescent Carbon Dots from Waste Expanded Polystyrene and Its Application in the Fluorimetric Detection of Au 3+ Ions in Aqueous Media, ACS Sustain. Chem. Eng. 6 (2018) 1627–1638. https://doi.org/10.1021/acssuschemeng.7b02852.

[35] Q. Li, Y. Gao, J. Shen, X. Mu, J. Wang, L. Ouyang, K. Chen, H. He, J. Pei, Q. Ren, S. Sun, H. Liu, L. Zhou, Y. Sun, W. Long, J. Zhang, X.D. Zhang, Catalase-like quantum dots of L-lysine polymerization as free radical scavengers for hypoxic brain injury, Mater. Today Commun. 27 (2021) 102286. https://doi.org/10.1016/j.mtcomm.2021.102286.

[36] X. Mu, H. He, J. Wang, W. Long, Q. Li, H. Liu, Y. Gao, L. Ouyang, Q. Ren, S. Sun, J. Wang, J. Yang, Q. Liu, Y. Sun, C. Liu, X.D. Zhang, W. Hu, Carbogenic nanozyme with ultrahigh reactive nitrogen species selectivity for traumatic brain injury, Nano Lett. 19 (2019) 4527–4534. https://doi.org/10.1021/acs.nanolett.9b01333.

[37] N. Alizadeh, A. Salimi, A. Salimi, A. Salimi, T.K. Sham, P. Bazylewski, G. Fanchini, Intrinsic Enzyme-like Activities of Cerium Oxide Nanocomposite and Its Application for Extracellular H2O2Detection Using an Electrochemical Microfluidic Device, ACS Omega. 5 (2020) 11883–11894. https://doi.org/10.1021/acsomega.9b03252.

[38] H. He, X. Shi, J. Wang, X. Wang, Q. Wang, D. Yu, B. Ge, X. Zhang, F. Huang, Reactive Oxygen Species-Induced Aggregation of Nanozymes for Neuron Injury, ACS Appl. Mater. Interfaces. 12 (2020) 209–216. https://doi.org/10.1021/acsami.9b17509.

[39] I.L. Christensen, Y.P. Sun, P. Juzenas, Carbon dots as antioxidants and prooxidants, J. Biomed. Nanotechnol. 7 (2011) 667–676. https://doi.org/10.1166/jbn.2011.1334.

[40] X.D. Zhang, L. Ouyang, X. Mu, J. Wang, Q. Li, Y. Gao, H. Liu, S. Sun, Q. Ren, R. Yan, J. Wang, Q. Liu, Y. Sun, C. Liu, H. He, W. Long, X.D. Zhang, Carbon dot targeting to nitrogen signaling molecules for inhibiting neuronal death, J. Mater. Chem. B. 8 (2020) 2321–2330. https://doi.org/10.1039/c9tb02447f.

[41] L. Zhao, M. Zhang, H. Wang, S. Devahastin, Effects of carbon dots in combination with

rosemary-inspired carnosic acid on oxidative stability of deep frying oils, Food Control. 125 (2021) 107968. https://doi.org/10.1016/j.foodcont.2021.107968.

[42] W. Feng, X. Han, H. Hu, M. Chang, L. Ding, H. Xiang, Y. Chen, Y. Li, 2D vanadium carbide MXenzyme to alleviate ROS-mediated inflammatory and neurodegenerative diseases, Nat. Commun. 12 (2021). https://doi.org/10.1038/s41467-021-22278-x.

[43] Y. Hu, X.J. Gao, Y. Zhu, F. Muhammad, S. Tan, W. Cao, S. Lin, Z. Jin, X. Gao, H. Wei, Nitrogen-Doped Carbon Nanomaterials as Highly Active and Specific Peroxidase Mimics, Chem. Mater. 30 (2018) 6431–6439. https://doi.org/10.1021/acs.chemmater.8b02726.

[44] S. Jung, I. Kwon, Synergistic degradation of a hyperuricemia-causing metabolite using one-pot enzyme-nanozyme cascade reactions, Sci. Rep. 7 (2017) 1–8. https://doi.org/10.1038/srep44330.

[45] R. Jain, M. Mathur, S. Sikarwar, A. Mittal, Removal of the hazardous dye rhodamine B through photocatalytic and adsorption treatments, J. Environ. Manage. 85 (2007) 956–964. https://doi.org/10.1016/j.jenvman.2006.11.002.

[46] J. Piella, F. Merkoçi, A. Genç, J. Arbiol, N.G. Bastús, V. Puntes, Probing the surface reactivity of nanocrystals by the catalytic degradation of organic dyes: The effect of size, surface chemistry and composition, J. Mater. Chem. A. 5 (2017) 11917–11929. https://doi.org/10.1039/c7ta01328k.

[47] P.C. Nagajyoyhi, K.C. Devarayapalli, T.V.M. Sreekanth, S.V.P. Vattikuti, J. Shim, Effective catalytic degradation of rhodamine B using ZnCO2O4 nanodice, Mater. Res. Express. 6 (2019) 0–6. https://doi.org/10.1088/2053-1591/ab3bbf.

[48] P. Saikia, A.T. Miah, P.P. Das, Highly efficient catalytic reductive degradation of various organic dyes by Au/CeO2-TiO2 nano-hybrid, J. Chem. Sci. 129 (2017) 81–93. https://doi.org/10.1007/s12039-016-1203-0.

[49] S. Zhou, L. Kong, C. Yan, Y. Zhou, X. Qiu, C. Liu, Rhodamine B dye is efficiently degraded by polypropylene-based cerium wet catalytic materials, RSC Adv. 10 (2020) 26813–26823. https://doi.org/10.1039/d0ra03965a.

[50] Y. Zhou, E.M. Zahran, B.A. Quiroga, J. Perez, K.J. Mintz, Z. Peng, P.Y. Liyanage, R.R. Pandey, C.C. Chusuei, R.M. Leblanc, Size-dependent photocatalytic activity of carbon dots with surface-state determined photoluminescence, Appl. Catal. B Environ. 248 (2019) 157–166. https://doi.org/10.1016/j.apcatb.2019.02.019.

[51] A. Mondal, B. Adhikary, D. Mukherjee, Room-temperature synthesis of air stable cobalt nanoparticles and their use as catalyst for methyl orange dye degradation, Colloids Surfaces A Physicochem. Eng. Asp. 482 (2015) 248–257. https://doi.org/10.1016/j.colsurfa.2015.05.011.

[52] S. Paul, S.L. Banerjee, M. Khamrai, S. Samanta, S. Singh, P.P. Kundu, A.K. Ghosh, Hydrothermal synthesis of gelatin quantum dots for high-performance biological imaging applications, J.

Photochem. Photobiol. B Biol. 212 (2020) 112014. https://doi.org/10.1016/j.jphotobiol.2020.112014.

[53] Z. Zhang, W. Sun, P. Wu, Highly Photoluminescent Carbon Dots Derived from Egg White: Facile and Green Synthesis, Photoluminescence Properties, and Multiple Applications, ACS Sustain. Chem. Eng. 3 (2015) 1412–1418. https://doi.org/10.1021/acssuschemeng.5b00156.

[54] D. Gu, S. Shang, Q. Yu, J. Shen, Green synthesis of nitrogen-doped carbon dots from lotus root for Hg(II) ions detection and cell imaging, Appl. Surf. Sci. 390 (2016) 38–42. https://doi.org/10.1016/j.apsusc.2016.08.012.